Thermal Stability, Structural Features and B-to-Z Transition in DNA Tetraloop Hairpins as Determined by Optical Spectroscopy in d(CG)(3)T-4(CG)(3)and d(CG)(3)A(4)(CG)(3) Oligodeoxy...

ARTICLE *in* BIOPOLYMERS · JUNE 2005

Impact Factor: 2.39 · DOI: 10.1002/bip.20246 · Source: PubMed

Belén Hernández
Université Paris 13 Nord

Vladimir Baumruk
Charles University in Prague

Mahmoud Ghomi
Université Paris 13 Nord

Belén Hernández[1]
Vladimir Baumruk[2]
Catherine Gouyette[3]
Mahmoud Ghomi[1]
[1] *UMR CNRS 7033, BioMoCeTi, Université Pierre et Marie Curie, Case 138, 4 Place Jussieu, 75252 Paris cedex 05, and UFR SMBH, Université Paris 13, 74 rue Marcel Cachin, 93017 Bobigny cedex, France*

Thermal Stability, Structural Features, and B-to-Z Transition in DNA Tetraloop Hairpins as Determined by Optical Spectroscopy in $d(CG)_3T_4(CG)_3$ and $d(CG)_3A_4(CG)_3$ Oligodeoxynucleotides

[2] *Institute of Physics, Charles University, Ke Karlovu 5, 12116 Prague 2, Czech Republic.*

[3] *Unité de Chimie Organique, Institut Pasteur, 28 rue du Docteur Roux, 75724 Paris cedex 15, France*

Received 12 October 2004; accepted 3 January 2005
Published online 2 February 2005 in Wiley InterScience (www.interscience.wiley.com). DOI 10.1002/bip.20246

Abstract: *NMR and CD data have previously shown the formation of the T_4 tetraloop hairpin in aqueous solutions, as well as the possibility of the B-to-Z transition in its stem in high salt concentration conditions. It has been shown that the stem B-to-Z transition in T_4 hairpins leads to S (south)- to N (north)-type conformational changes in the loop sugars, as well as* anti *to* syn *orientations in the loop bases. In this article, we have compared by means of UV absorption, CD, Raman, and Fourier transform infrared (FTIR), the thermodynamic and structural properties of the T_4 and A_4 tetraloop hairpins formed in 5′-d(CGCGCG-TTTT-CGCGCG)-3′ and 5′-d(CGCGCG-AAAA-CGCGCG)-3′, respectively. In presence of 5*M *$NaClO_4$, a complete B-to-Z transition of the stems is first proved by CD spectra. UV melting profiles are consistent with a higher thermal stability of the T_4 hairpin compared to the A_4 hairpin. Order-to-disorder transition of both hairpins has also been analyzed by means of Raman spectra recorded as a function of temperature. A clear Z-to-B transition of the stem has been confirmed in the T_4 hairpin, and not in the A_4 hairpin. With a right-handed stem, Raman and FTIR spectra have confirmed the C2′*-endo/anti *conformation for all the T_4 loop nucleosides. With a left-handed stem, a part of the T_4 loop sugars adopt a N-type (C3′*-endo*) conformation, and the C3′*-endo/syn *conformation seems to be*

Correspondence to: Mahmoud Ghomi; email: ghomi@ccr.jussieu.fr and ghomi@smbh.univ-paris13.fr

Biopolymers, Vol. 78, 21–34 (2005)

the preferred one for the dA residues involved in the A_4 tetraloop. Biopolymers 78: 21–34, 2005

This article was originally published online as an accepted preprint. The "Published Online" date corresponds to the preprint version. You can request a copy of the preprint by emailing the Biopolymers editorial office at biopolymers@wiley.com

Keywords: *hairpins; DNA folding; oligodeoxynucleotides; optical spectroscopy*

INTRODUCTION

DNA hairpins were found to play an important role in gene transcription and replication regions.[1–9] Palindromes, or DNA sequences with inverted repeats, are capable of forming cruciform structures,[5] containing two intrastrand hairpins on each side of a double-stranded DNA. Generation of a cruciform is supposed to be responsible for the torsional stress relaxation in negatively supercoiled plasmids.[6–10] Influence of DNA secondary structure on its interaction with enzymes has been previously discussed.[11–13] Moreover, folded regions of nucleic acids are their most exposed parts to the solvent and surrounding molecules, explaining the privileged role of DNA (or RNA) hairpins in intermolecular recognition and interactions with regulatory proteins and enzymes.[14,15] On the other hand, in the framework of gene therapy, antisense oligodeoxynucleotides have been currently conjugated to ultrastable hairpins in order to increase their stability against cellular nucleases.[16,17]

A DNA hairpin can be defined as an intramolecular double helix (*stem*) normally stabilized by canonical base pairs or mispairs, and capped by a number of unpaired or paired nucleosides (*loop*). The structural and thermodynamic stability of a hairpin is dependent on loop and stem base composition, loop and loop-over-stem base stacking, hydrogen bonds in the loops, closing base pair of the loop and length of the stem.[18,19]

Optical and chirooptical techniques such as UV absorption and CD are well adapted to provide information on the thermal stability and global structural features, e.g., thermodynamic parameters of a hairpin as well as the handedness (right or left) of its stem (vide infra). Vibrational spectroscopy can also provide the same kind of information as UV and CD experiments. It also yields useful structural data at nucleotide level in both DNA and RNA single and double strands, i.e., N- and S-type sugar puckering, *syn* and *anti* orientation of the bases, interbase hydrogen bonds, and base stacking. In fact, in many cases, the data provided by optical spectroscopy[20–27] can complement very well those obtained by NMR in solution. One of the significant roles played by optical spectroscopy in the field of nucleic acid structure is related to the first observations on the well-known B-to-Z (right-to-left handed) double-helical transition in DNA. This interesting basic phenomenon was evidenced by means of CD[20] and Raman[21] spectroscopies in aqueous solutions of polyd(G-C) upon increasing ionic strength, e.g., by varying the NaCl concentration in buffer from 100 m*M* (B form) to 4*M* (Z form). As far as the analysis of the thermal stability and structural features of folded nucleic chains are concerned, our group has published a series of investigations on the structural analysis of RNA ultrastable tetraloop hairpins by means of optical spectroscopy (UV, FTIR, Raman) and NMR. These studies were focused on the short oligoribonucleotides (octamers and decamers) capable of forming hairpins containing the most occurring tetraloops in 16S rRNAs, i.e., -UNCG-[28–32] and -GNRA-[32–34] (N is any nucleotide and R is a purine). In the present work, we aim to extend our investigations to stable DNA hairpins. Among all possible hairpins, we have chosen two of them containing -TTTT- (homopyrimidine) and -AAAA- (homopurine) tetraloops.

The choice of the -TTTT- (hereafter referred to as T_4) tetraloop is related to the fact that it is one of the most documented and perhaps the unique one for which we find a substantial amount of thermodynamic and structural data in the literature.[35–42] The analysis of the T_4 tetraloop hairpin was started by a systematic optical analysis of d(ATCCTA-T_n-TAGGAT) oligomers,[35] with $n = 1$–5.[35,36] It was shown that for $n = 1$, the oligomer adopts a double-helical (dimer) form, whereas for $n = 2$ an equilibrium is found between dimers and monomers (hairpins with six base pairs in each stem). Only hairpins (monomers) appear in solution when $n = 3$–5. Another work by means of NMR[36] has been undertaken on the above-mentioned generic sequence but with $n = 4$–7. Particularly, T-jump and UV absorption measurements have revealed that the thermal stability of these hairpins decreases when n increases. In these studies, $n = 4$ was found to be the optimal number for T_n loops in regard to their thermal stability. A series of other valuable publications have described the formation of T_4 tetraloop hairpins in $d(CG)_mT_4(CG)_m$ sequences, with $m = 2$, 3, and 5.[37–42] In fact, the idea was to induce a B-to-Z form transition in the stem of these hairpins. This explains the choice of d(CG)$_m$ stems, which was undoubtedly related to the Z-form double-helix observations in the crystal structure of d(CG)$_3$ in 1979.[43] Another objective was to understand the influence of the T_4 tetraloop on the whole structure and stability of hairpins. The main results of this series of investigations can be briefly described as follows:

- In all cases the presence of the tetraloop leads to a considerable increase of thermal stability compared to that measured in a reference double helix containing the same base repeat as in the stem of hairpins. As previously mentioned,[40] the added stability of the hairpin is of entropic origin.
- Based on UV and NMR results,[37] the stem of d(CG)$_5$T$_4$(CG)$_5$ hairpin undergoes a B-to-Z form transition in particular conditions: high concentration of Na^+ or Mg^{2+} and dehydration (ethanol) conditions.
- NMR results have shown that the oligomer d(CG)$_2$T$_4$(CG)$_2$ forms a tetraloop hairpin with a B form stem.[38] The use of distance geometry calculations have permitted the obtention of the T_4 tetraloop hairpin three-dimensional (3D) structure (up to now the only existing structural model of this hairpin in solution). Figure 1 displays a schematic representation of this hairpin.
- Optical spectroscopy and NMR could prove the formation of a T_4 hairpin (with a stem in B form containing six GC base pairs) in aqueous solutions of d(CG)$_3$T$_4$(CG)$_3$.[39] By following the procedure reported by Xodo et al.[44–46] for the T_5 and A_5 pentaloop haipins, Benight et al.[40] have shown that the stem of the hairpin d(CG)$_3$ T$_4$(CG)$_3$ can also undergo a B-to-Z transition in buffers containing 4*M* $NaClO_4$. This was the first time that a T_4 hairpin could be identified in solution with a short left-handed stem (six GC base pairs).
- All these studies have led Chattopadhyaya et al.[41,42] to resolve the crystal structure of a T_4 hairpin with a Z-form stem, observed in the hexadecamer d(CG)$_3$T$_4$(CG)$_3$. This crystal structure is displayed schematically in Figure 1 and compared to the solution hairpin structure with a B-form stem[38] (described above). The structural characteristics of the Z-form stem are similar to those observed ten years before in d(CG)$_3$ double helix.[43] The most surprising effect was the 3D structure of the T_4 tetraloop in crystal phase: the ultimate 3′- and 5′ thymine bases are looped out, whereas the two middle thymines are stacked together and parallel to the double-helix axis. The looped-out position of the loop ultimate thymine bases makes possible intermolecular interaction by formation of the T · T mispair between two neighboring hairpins in the crystal lattice.

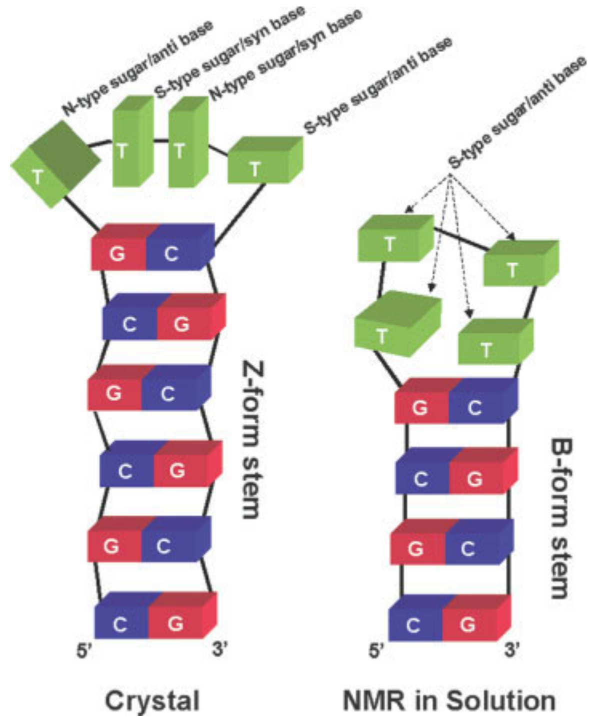

FIGURE 1 Schematic representations of the T_4 hairpins with B-form and Z-form stems. Right: B-form stem. Structural model proposed from the distance geometry calculations based on the NMR data collected in the low salt aqueous solutions of the dodecamer d(CG)$_2$T$_4$(CG)$_2$.[38] Left: Z-form stem. Structural model constructed from the diffraction data collected on the crystal form of the hexadecamer d(CG)$_3$T$_4$(CG)$_3$.[41,42]

In contrast to T_4 hairpins, no data of this type is available on A_4 hairpins. The only available data are those reported by Xodo et al.[45,46] on the A_5 hairpin with both B- and Z form stems (Table I). To our knowledge, no vibrational data is available for T_4 and A_4 hairpins. The present article contributes to the elucidation of the thermodynamic and structural features of these two hairpins by means of optical techniques such as UV absorption, CD, Fourier transform infrared (FTIR) absorption, and Raman scattering.

EXPERIMENTAL

Sample Preparation

The two hexadecamers, 5′-d(CGCGCG-TTTT-CGCGCG)-3′ and 5′-d(CGCGCG-AAAA-CGCGCG)-3′ analyzed in this work, hereafter referred to as T_4 and A_4 hairpins (or tetraloops) (Table I), were synthesized with one NH_4^+ per phosphate group at the Institut Pasteur, Paris, France (T_4 hairpin) and at the laboratory of Plant Molecular Physiology, Masaryl University, Brno, Czech Republic (A_4 hairpin). Initial lyophilized powder samples were dissolved in phosphate buffer, pH = 6.8, containing 10 m*M* monovalent cations (Na^+ and K^+) and 1 m*M* EDTA, to obtain aqueous samples used for optical spectroscopy. Stock solutions of each oligomer at $C_{oligomer}$ = 5 m*M* were first prepared and directly used for Raman and FTIR measurements. They were further diluted to obtain solutions with $C_{oligomer}$ = 20 and 100 μM for recording both UV absorption and CD spectra. Following previous works on the T_4 and T_5 hairpins,[40,44,46] a progressive B-to-Z conformational transition was induced in the stem of hairpins by adding an increasing amount of $NaClO_4$, up to 5*M*, to the phosphate buffer containing one of the oligomers. Raman and FTIR spectra were recorded at 5*M* $NaClO_4$, where the formation of Z-form stems was completely achieved (vide infra).

Spectroscopic Measurements

UV absorption melting profiles at 280 nm were obtained using an UVIKON XL spectrophotometer with a multisample holder, equipped with a Pelletier heating accessory. Cuvettes with 3 or 4 mm optical pathlengths, containing oligomer samples, were first heated from room temperature to 90°C and then cooled down in order to assure the formation of hairpins in solution. UV absorption melting profiles were measured between 10 and 90°C in phosphate buffer and between 10 and 70°C in presence of $NaClO_4$ (heating or cooling rate was 0.5°C/min). The reversibility of melting profiles has been verified for each hairpin. Thermodynamic parameters such as T_m, $\Delta H°$ and $\Delta S°$ (where T_m = melting temperature, $\Delta H°$ = variation in enthalpy and $\Delta S°$ = variation in entropy) in going from an ordered initial state (hairpin) to a disordered (random coil) structure, were calculated using the theoretical model described pereviously.[47] In this model, the variation of normalized optical density (NOD) at low temperature (hairpin state) and high temperature (disordered state) are supposed to be linear vs. temperature. Between these two states, a sigmoidal function depending on $\Delta H°$ and $\Delta S°$ gives the variation of NOD as a function of temperature. The model depends consequently on six parameters to be determined on the basis of melting curve fitting. Initial guess of T_m is estimated by second derivative calculation of the observed melting curve, whereas the fitting procedure provides it final value. However, in all the fits performed in the framework of this work, initial and final T_m values remained very close one to another.

CD spectra of T_4 and A_4 hairpins were recorded on a JASCO J-810 spectrophotometer equipped with a Pelletier accessory. Two millimeters pathlength quartz cells containing 600 μL of sample solution were used. CD spectra of both hairpins in presence of 5*M* $NaClO_4$ were collected from 10 to 70°C by successive steps of 10°C. Thermal equilibration was assured by maintaining the sample for 5 min at each temperature.

FTIR spectra were recorded at room temperature with a Nicolet Magna 860 spectrometer using a standard source, a CsI beamsplitter, and a liquid nitrogen cooled MCT detector. Usually 500 scans were collected with 2 cm^{-1} spectral resolution and a Happ–Genzel apodization function. Samples were placed in a demountable press-lock cell consisting of a pair of ZnSe windows and a 25-μm teflon spacer.

Raman spectra were excited at 488 nm with an Ar^+ laser (Stabilite model 2017-04S, Spectra Physics) and collected on a Jobin-Yvon T64000 spectrograph in a single spectrograph configuration with a 1200-groove/mm holographic grating and a holographic notch filter. The spectrograph is equipped with a liquid nitrogen cooled CCD detection system (Spectrum One, Jobin-Yvon) based on a Tektronix CCD chip of 2000 × 800 pixels. The effective spectral slit width was set to ca. 5 cm^{-1}. Raman spectra were collected from 10 to 90°C in phosphate buffer, and within 10 to 70°C in $NaClO_4$. Postprocessing (subtraction of buffer contribution, baseline correction, and smoothing) of all spectral data were performed using GRAMS/32 software (Galactic Industries). Following the considered sample, buffer contribution, also recorded as a function of temperature, was subtracted in two different manners: (i) For the spectra recorded in phosphate buffer, both spectra (from oligomer and buffer) were first normalized to the water angular bending mode at 1645 cm^{-1} before subtraction. (ii) In the case of samples containing $NaClO_4$, both spectra were normalized first to the very intense 937-cm^{-1} Raman band assigned to ClO_4^- ions (much more intense than the water reference). To subtract the buffer spectrum from the oligomer spectrum, a special attention was also paid to remove as accurately as possible another intense band arising from ClO_4^- ions, located at 630 cm^{-1}, very close to the Z form Raman marker. To compute the difference Raman spectra recorded at two different temperatures, they were both normalized to the routinely used nucleic acid internal reference, i.e., the PO_2^- symmetric stretch band at ca. 1093 cm^{-1}. Spectra shown in this article have been drawn using the SIGMAPLOT package.

RESULTS AND DISCUSSION

UV and CD Spectra

Thermal Stability of Hairpins and B-to-Z Transition of Stems. In phosphate buffer, UV absorption melting profiles are shown to be independent of oligomer concentration in the 50–200 μL range (Figure 2). The high thermal stability of these hairpins has been proved by their T_m values as reported in Table 1 (80.7 and 76.6°C for the T_4 and A_4 hairpins, respectively). CD spectra of both hairpins obtained at 20°C reveal, as expected, the existence of B-form stems, as characterized by a negative band at ca. 255 nm and a positive one at ca. 277 nm (Figure 2). It should be pointed out that a difference of ca. 6°C between the

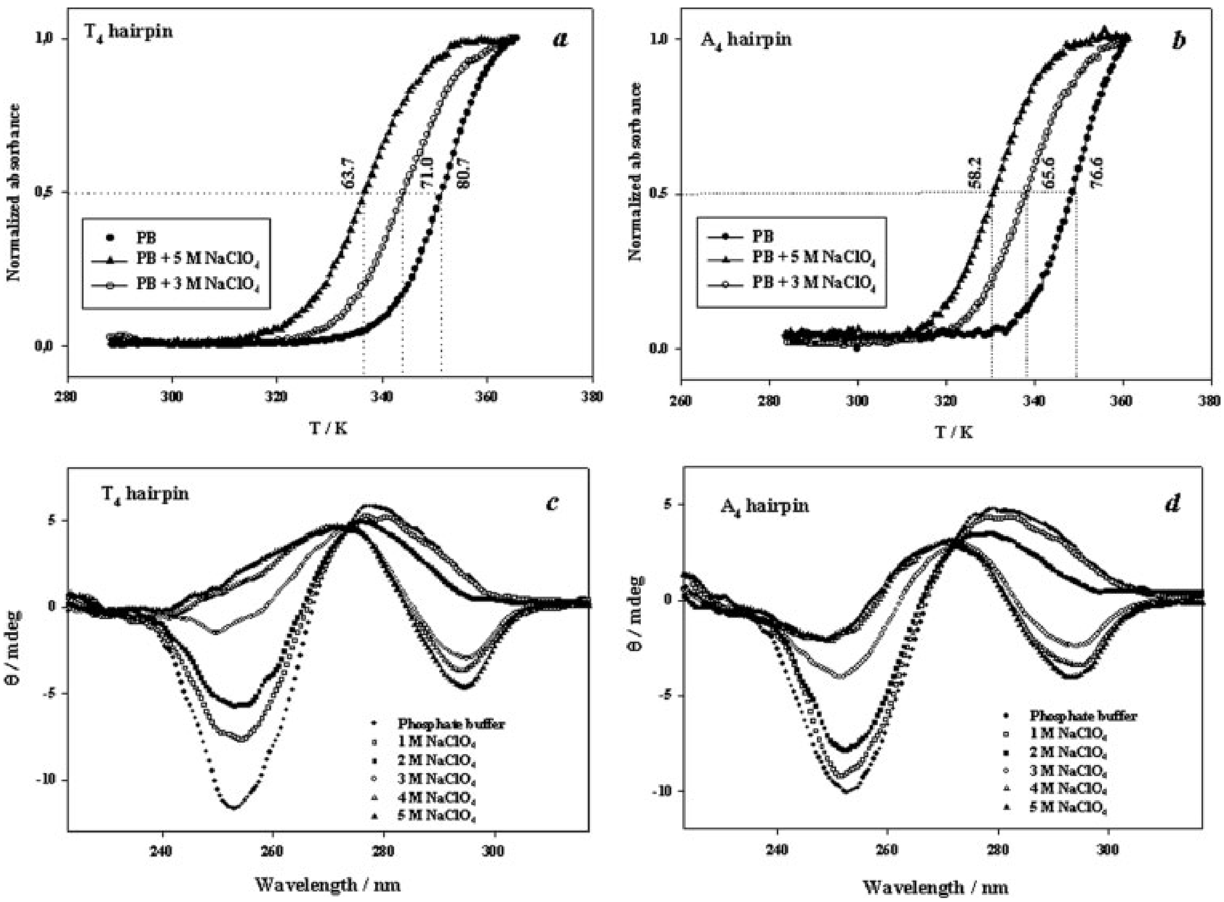

FIGURE 2 UV absorption melting profiles (a and b) and CD (c and d) spectra obtained from the T_4 (a and c) and A_4 (b and d) hairpins formed in different solvents. Oligonucleotide concentration was 20 μM at pH = 6.8. Note that the UV absorption melting profiles are identical in the 50–200-μL oligomer concentration range. Obtained initially in phosphate buffer (PB), the melting profiles show a gradual decrease of T_m (melting temperature) upon addition of $NaClO_4$ (see also Table I), while CD spectra taken at room temperature show a gradual signal inversion consistent with a B-to-Z conformational transition in the stem of both hairpins. The formation of hairpins with a Z-form stem is complete for 5*M* of sodium perchloride in buffer solution.

T_m of the T_4 hairpin, as reported here and in Ref. 40, is mainly due to a higher ionic strength used in previous measurements (phosphate buffer + 100 m*M* NaCl).

Upon addition of $NaClO_4$, two distinct phenomena are observed: (i) a progressive decrease of the T_m value for both hairpins (Figure 2, top), (ii) a progressive inversion of the CD signal measured at 20°C, confirming a gradual B-to-Z conformational transition in the stems (Figure 2, bottom). This transition is complete at 5*M* $NaClO_4$ as proved by the Z-form CD signatures, i.e., a positive band at ca. 272 nm followed, in its high wavelength side, by a negative one at ca. 294 nm (Figure 2, bottom).

Note the existence of isoelliptic points observed in CD spectra confirming the B-to-Z transition in the stems of the T_4 (Figure 2c) and A_4 (Figure 2d) hairpins.

Previous measurements[40] have shown that the Z-form completion in the stem of the T_4 hairpin can be observed in presence of 100 m*M* NaCl + 4*M* $NaClO_4$ (Table I). Our experiments, performed without NaCl added to the buffer, needed a higher $NaClO_4$ concentration (5*M*) to complete the B-to-Z transition. As estimated from the values reported in Table I, $\Delta T_{m(B\text{-}Z)} = 17°C$ in the T_4 hairpin (in agreement with previous measurements,[38] Table I) and $\Delta T_{m(B\text{-}Z)} = 18.4°C$ in the A_4 hairpin. A ΔT_m = 5.5°C has been estimated (Table I) between the two hairpins with Z-form stems. Thus, whatever the handedness of the stem (right or left), the T_4 hairpin is more stable than the A_4 hairpin. We assign this effect to the base stacking in the loops, and to a lesser extent to the closing base pair (GC in both hairpins).

Table I Thermodynamic Parameters of the Oligomers Capable of Forming T_4, T_5, A_4, and A_5 Hairpins in Solution with a Stem Constituted by Six CG Base Pairs[a]

Oligomers	Solvent	Conformation in Solution UV and CD Spectra	Hairpin Thermodynamic Parameters UV Absorption Melting Profiles			References
			T_m	$\Delta H°$	$\Delta S°$	
5′-d(CGCGCG-TTTT-CGCGCG)-3′	PB	T_4 hairpin with a B-form stem	80.7	48.60	137.3	Present work[b]
	PB + 5*M* $NaClO_4$	T_4 hairpin with a Z-form stem	63.7	40.40	120.0	Present work[b]
5′-d(CGCGCG-AAAA-CGCGCG)-3′	PB	A_4 hairpin with a B-form stem	76.6	46.80	133.9	Present work[b]
	PB + 5*M* $NaClO_4$	A_4 hairpin with a Z-form stem	58.2	36.50	110.4	Present work[b]
5′-d(CGCGCG-TTTT-CGCGCG)-3′	PB + 100 m*M* NaCl	T_4 hairpin with a B-form stem	86.52	50	139	Ref. 40
	PB + 100 m*M* NaCl + 4*M* $NaClO_4$	T_4 hairpin with a Z-form stem	64.08	45	133	Ref. 40
5′-d(CGCGCG-TTTTT-CGCGCG)-3′	0.5 m*M* Tris + 0.5 m*M* $NaClO_4$	Biphasic (duplex + T_5 hairpin with a B-form stem)	69	57	166	Ref. 45
	0.5 m*M* Tris + 4.6 *M* $NaClO_4$	T_5 hairpin with a Z-form stem	65	52	154	Refs. 44 and 46
5′-d(CGCGCG-AAAAA-CGCGCG)-3′	0.5 m*M* Tris + 0.5 m*M* $NaClO_4$	Biphasic (duplex + A_5 hairpin with a B-form stem)	68	55	162	Ref. 45
	0.5 m*M* Tris + 4.6*M* $NaClO_4$	A_5 hairpin with a Z-form stem	67	52	153	Refs. 44 and 46
Reference duplex 5′-d(CGCGCG)-3′	PB + 100 m*M* NaCl	B-form double helix	43.25	50	161	Ref. 38
	PB + 100 m*M* NaCl + 4*M* $NaClO_4$	Z-form double helix	25.71	45	151	Ref. 38

[a] In the primary sequences, the underlined bases are those forming the hairpin loops. The other bases form an intermolecular $d(CG)_3$ double helix (stem) stabilizing the whole tetraloop hairpin. PB: phosphate buffer with very low salt concentration (10 m*M* of Na^+ and/or K^+ counterions). B-form: right-handed double helix (stem of the hairpins in low salt solutions). Z-form: left-handed double helix (stem of the hairpins in high salt solutions). Thermodynamic parameters (and their units) are derived from a two state model: T_m, melting temperature, (°C); $\Delta H°$, variation in enthalpy, (kcal · mol^{-1}); $\Delta S°$, variation in entropy, (cal · mol^{-1} · K^{-1}).

[b] Estimated errors for thermodynamic parameters: T_m (± 0.5° C). ΔH° and ΔS° (± 5% of reported values).

Raman and FTIR Spectra

In Figures 3–5 are shown the Raman spectra of the T_4 and A_4 hairpins as a function of temperature. To assign the observed vibrational modes to the nucleosides or to the phosphate backbone, we have been inspired either from the published vibrational spectra of $d(CG)_3$,[22] polyd(G-C),[23] polydA, and polyd(A-T),[25] or from the review articles devoted to the analysis of DNA polymorphism by means of Raman spectroscopy.[48] The use of the above-mentioned reference spectra helped us to assign with more confidence the vibrational modes observed in the hairpins (Table II). Figures 6 and 7 display band decomposition of Raman spectra in the spectral region mainly involving vibrational motions from nucleosides.

Vibrational Markers Arising from the Stems of the T_4 and A_4 Hairpins. In a B-form double helix, all nucleosides have a C2′-*endo*/*anti* conformation. A glance of the Raman spectra observed in phosphate buffer (Figures 3 and 4) allows us to recognize a set of

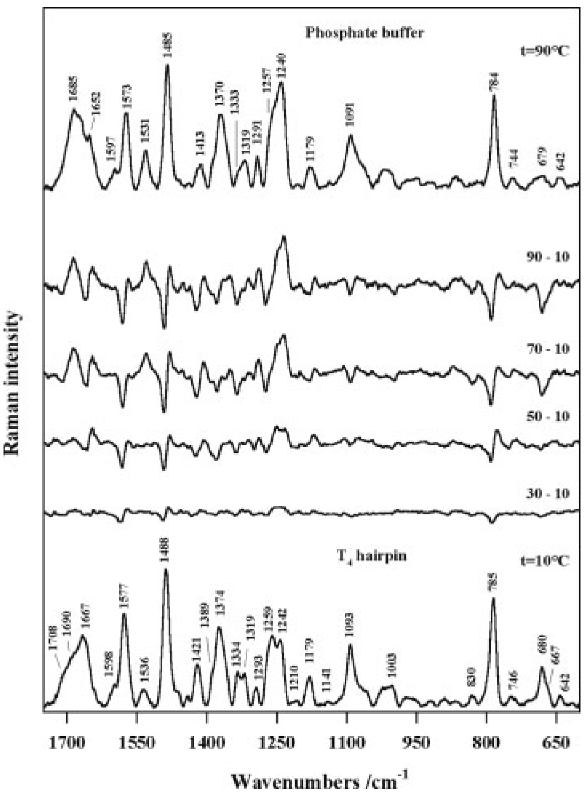

FIGURE 3 Raman spectra of the T_4 hairpin (with a B-form stem) formed in phosphate buffer. Oligonucleotide concentration was 5 m*M* at pH = 6.8. Exciting wavelength 488 nm. Bottom: Raman spectrum at 10°C. Top: Raman spectrum at 90°C. Between these two spectra are displayed the difference Raman spectra obtained for each one by subtracting the 10°C Raman spectrum from that corresponding to a higher temperature as indicated.

Raman bands corresponding to a B-form stem: (i) at ca. 680 cm^{-1} relative to C2′-*endo*/*anti* dG residues, (ii) at 1259 cm^{-1} (intense band) and at ca. 1269 cm^{-1} (shoulder) corresponding to C2′-*endo*/*anti* dC residues, (iii) at ca. 830 cm^{-1} arising from a B-form phosphate backbone. Similarly, the left-handed (Z-form) conformation of the stems can be confirmed by the Raman markers observed in presence of 5*M* $NaClO_4$ (Figures 4 and 5). We recall that in a Z-form double helix, pyrimidine nucleosides have a C2′-*endo*/*anti* conformation, whereas purine nucleosides adopt a C3′-*endo*/*syn* conformation. The C3′-*endo*/*syn* conformation of the dG residues in the stems is evidenced by first a notable increase of the Raman band at 1319 cm^{-1} (Figures 3–7), and then by a considerable downshift of the G breathing mode to ca. 630 cm^{-1}. The C2′-*endo*/*anti* conformation of the dC residues is now confirmed with an intense and well-resolved band observed at ca. 1263 cm^{-1} (Figures 3–4 and 6–7).

To enlarge the scope of our investigations on the stem B-to-Z transition, we switch to FTIR spectra (Figures 8 and 9), which are very well adapted to analyze the type of sugar puckering. Generally, C3′-*endo* (N-type) and C2′-*endo* (S-type) FTIR markers are observed at ca. 805 and 830 cm^{-1}, respectively. Both N- and S-type sugars are present in a Z-form double helix. This fact can be confirmed by FTIR spectra recorded in the presence of 5*M* $NaClO_4$ (Figure 9), where a set of bands are observed between 840 and 800 cm^{-1}. In contrast,

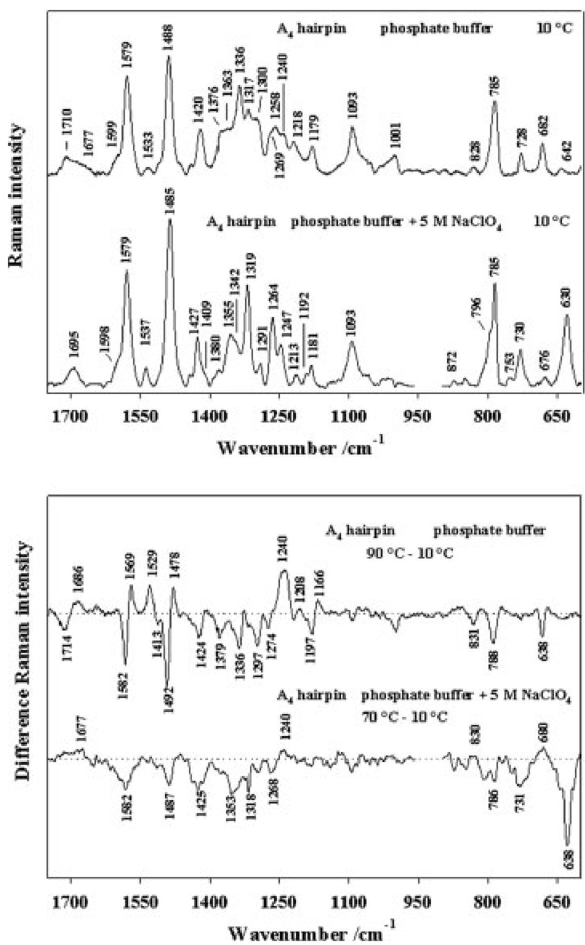

FIGURE 4 Raman and difference Raman spectra of the A_4 hairpin formed in different solvents. Oligonucleotide concentration was 5 m*M* at pH = 6.8. Exciting wavelength 488 nm. Top: Raman spectra obtained at 10°C in phosphate buffer, and after addition of 5*M* $NaClO_4$. The 1000–900-cm^{-1} spectral region containing the very intense $NaClO_4$ Raman line at 937 cm^{-1}, has been skipped in the Raman spectra obtained in presence of sodium perchloride. Bottom: Difference Raman spectra obtained by subtracting the 10°C Raman spectrum from that corresponding to the highest temperature, i.e., 90°C in phosphate buffer and 70°C in phosphate buffer + 5*M* $NaClO_4$.

Table II Wavenumbers and Tentative Assignments of the Vibrational Modes Observed at Room Temperature in the T_4 and A_4 Tetraloop Hairpins with the Stems in B and Z Double-Helical Conformations[a]

T_4 Hairpin B-Form Stem		A_4 Hairpin B-Form Stem		T_4 Hairpin Z-Form Stem		A_4 Hairpin Z-Form Stem		
Raman	FTIR	Raman	FTIR	Raman	FTIR	Raman	FTIR	Tentative Assignments
1708 (sh)		1710 (m)				1695 (m)		G ring; C═O bond stetch; stem
1690 (sh)				1687 (s)				T ring; C═O bond stretch; T_4 loop
1667 (s)		1677 (sh)		1666 (s)				T ring; planar mode; stem
				1645 (sh)				C ring; planar mode; stems
1598 (sh)		1599 (sh)		1602 (sh)		1598 (sh)		C ring; planar mode; stems
1577 (s)		1579 (s)		1578 (s)		1579 (s)		G and C rings; planar modes; stems
1536 (w)	1529 (m)	1533 (w)	1529 (m)	1537 (m)	1530 (w)	1537 (w)	1530 (m)	C and G; planar modes; stems
	1495 (m)		1497 (m)		1494 (m)		1495 (s)	C; planar mode; stems
1488 (s)		1488 (s)		1486 (s)		1485 (s)	1485 (sh)	G and A rings; planar modes; stems and loop
	1459 (m)		1459 (m)		1452 (m)		1457 (sh)	backbone; sugar
	1443 (m)		1445 (sh)		1441 (m)		1444 (s)	backbone; sugar
1421 (m)	1420 (m)	1420 (m)	1421 (m)					backbone; *B-helix marker*
				1425 (m)		1427 (m)	1430 (sh)	backbone; *Z-helix marker*
				1415 (sh)	1411 (sh)	1409 (w)	1408 (m)	backbone; *A-helix marker, C3′-endo/anti marker*
1389 (sh)	1390 (w)		1391 (w)	1388 (sh)	1387 (w)	1380 (w)	1387 (w)	G ring; planar mode; stems; *Ordered chain marker*
1374 (s)		1376 (m)		1374 (s)				dT and dA; loops
	1374 (m)		1374 (m)					dG; stems; *C2′-endo/anti marker (B-helix)*
		1363 (sh)		1360 (sh)				dG; stems
					1364 (w)		1364 (m)	dC; stems
						1355 (m)		dA; A_4 loop
	1358 (w)				1353 (sh)		1356 (m)	dG; *C3′-endo/syn marker (Z-helix)*
1334 (m)		1336 (s)	1335 (w)			1342 (sh)		dG and dA; stems and A_4 loop
1319 (m)	1325 (w)	1317 (s)		1319 (s)	1321 (w)	1319 (s)	1320 (m)	dG and dA; stems and A_4 loop; *increase in Z-helix*
1293 (w)	1295 (m)	1300 (s)	1296 (m)	1291 (w)	1292 (w)	1291 (w)	1292 (w)	dC and dA; stems and A_4 loop
	1281 (m)				1284 (w)			dC; stems
1268 (sh)		1269 (sh)		1263 (s)	1263 (w)	1264 (s)	1264 (w)	dC; stems; *C2′-endo/anti marker (B- and Z-helices)*
1259 (s)		1258 (m)						dC and dA; stems and A_4 loop
1242 (s)		1240 (m)		1245 (s)		1247 (m)		dC and dT; stems and T_4 loop
	1222 (s)		1223 (s)		1216 (s)		1219 (s)	PO_2^- anti-symmetric bond stretch; *helix marker*

Table II (*Continued from the previous page*)

T_4 Hairpin B-Form Stem		A_4 Hairpin B-Form Stem		T_4 Hairpin Z-Form Stem		A_4 Hairpin Z-Form Stem		
Raman	FTIR	Raman	FTIR	Raman	FTIR	Raman	FTIR	Tentative Assignments
		1218 (m)		1210 (w)		1213 (w)		dG and dT; stems and T_4 loop
1179 (m)		1179 (m)		1181 (m)		1181 (m)		dG; stems
1093 (s)		1093 (s)		1093 (s)		1093 (m)		PO_2^-; symmetric bond stretch
1022 (w)			*1018 (s)*		*1012 (m)*		*1014 (s)*	backbone; sugar
1003 (w)		1001 (w)						backbone; sugar
	971 (s)		*970 (s)*		*968 (s)*		*968 (s)*	Phosphate–backbone
					951 (m)		*951 (sh)*	Phosphate–backbone; *increase in Z-helix IR spectra*
	937 (m)		*934 (w)*					Phosphate–backbone
	920 (sh)		*921 (sh)*		*927 (s)*		*926 (m)*	Phosphate–backbone; *increase in Z-helix IR spectra*
	896 (m)		*895 (m)*		*893 (w)*		*893 (m)*	Phosphate–backbone
	852 (w)				*873 (m)*	872 (w)	*873 (m)*	Phosphate–backbone
830 (w)	*834 (w)*	828 (w)	*830 (w)*	831 (w)	*838 (m)*		*839 (m)*	Phosphate–backbone; *S-type sugar marker*
	828 (w)				*831 (sh)*			
					801 (m)		*805 (sh)*	Phosphate–backbone; *N-type sugar marker*
			798 (s)			796 (sh)	*798 (m)*	dA residue; A_4 loop
785 (s)		785 (s)		785 (s)		785 (s)		dC; C ring breathing mode; stems
					786 (s)		*786 (m)*	G and C; ring out-of-plane modes; stems
	780 (s)		*780 (s)*		*780 (m)*		*780 (m)*	
	770 (sh)				*771 (sh)*			Phosphate–backbone
	760 (sh)				*756 (m)*	753 (w)		Phosphate–backbone
746 (w)				746 (w)	*746 (m)*		*747 (w)*	dT, T ring breathing mode; loop; *C2′-endo/anti marker*
		728 (m)			*732 (m)*	730 (m)	*732 (w)*	dA, A ring breathing mode; loop
				720 (w)				Phosphate–backbone
680 (m)		682 (m)				676 (w)		dG, G ring breathing mode; stems; *B-helix marker*
667 (sh)								dT; T_4 loop; *C2′-endo/anti marker*
642 (w)		642 (w)						dT and dA; loop
				636 (s)		630 (s)		dG, G ring breathing mode; stem; *Z-helix marker*

[a] In parentheses: s, strong; m, medium; w, weak; sh, shoulder. B-form stem: Raman spectra recorded in phosphate buffer. Z-form stem: Raman spectra recorded in phosphate buffer + 5*M* $NaClO_4$. *Italic numbers:* FTIR band wavenumbers observed in D_2O.

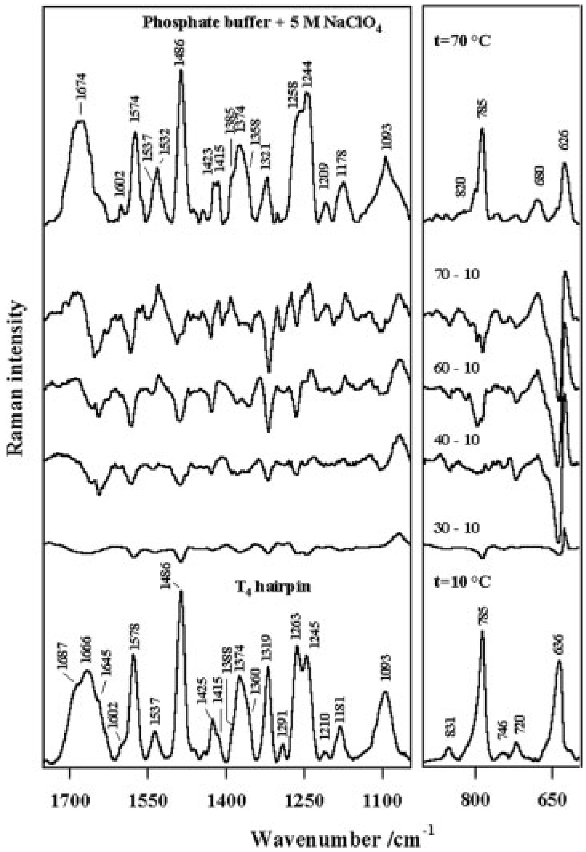

FIGURE 5 Raman spectra of the T_4 hairpin (with a Z-form stem) formed in phosphate buffer to which 5*M* $NaClO_4$ was added. Oligonucleotide concentration was 5 m*M* at pH = 6.8. Exciting wavelength: 488 nm. The 1000–900-cm^{-1} spectral region containing the very intense $NaClO_4$ Raman line at 937 cm^{-1} has been skipped. Bottom: Raman spectrum at 10°C. Top: Raman spectrum at 70°C. Between these two spectra are displayed difference Raman spectra obtained for each one by subtracting the 10°C Raman spectrum from that corresponding to a higher temperature.

FTIR spectra recorded in phosphate buffer (B-form stems) show only bands corresponding to C2′-*endo* sugars. Figure 8 shows the downshift of the FTIR bands from ca. 1420 cm^{-1} (B-form stems) to ca. 1410 cm^{-1} (Z-form stems). In Figure 8 can also be observed the behavior of another well-known dG residue vibrational mode, sensitive to B-to-Z transition. This band at 1374 cm^{-1} (B-form stems) is downshifted to 1356 cm^{-1} (A_4) and 1353 cm^{-1} in (T_4) (Z-form stems). Note also in FTIR spectra (Figures 8 and 9), the slight downshift of the PO_2^- asymmetric stretch vibration from ca. 1222 (B form) to 1216 cm^{-1} (Z form), as well as the increase in the intensity of the band at ca. 1014 and 930 cm^{-1}, all characteristic of the B-to-Z transition.[27]

Melting of Hairpins as Evidenced by Raman Spectra. Difference Raman spectra shown in Figures 3–5 allow us to account for a very valuable effect called *Raman hypochromism*, as well as for Raman band wavenumber shifts upon melting. Each difference spectrum is computed by subtracting the Raman spectrum at 10°C from that obtained at higher temperatures. Raman hypochromism observed as a function of temperature mainly indicates the loss of base stacking in both the loop and the stem of hairpins. Hypochromic effect is more pronounced in the hairpins with B form stems (Figures 3–5). This should be undoubtedly due to the difference between the base stacking in the B and Z forms.[43] In B-form stems, Raman hypochromism is mainly observed for the Raman bands arising from dC (785 cm^{-1}) and dG residues (ca. 1577, 1488, and 680 cm^{-1}). Melting effect in B-form stems can also be evidenced by the gradual disappearance of B-helix markers: bands at 830 cm^{-1} (phosphate-backbone), 1268 cm^{-1} (dC: C2′-*endo*/*anti*). In Z-form stems, the most hypochromic bands are those from dG (at ca. 1578, 1485, 1319, and 630 cm^{-1}) and dC (at ca. 1263 and 785 cm^{-1}) modes, upon increasing temperature.

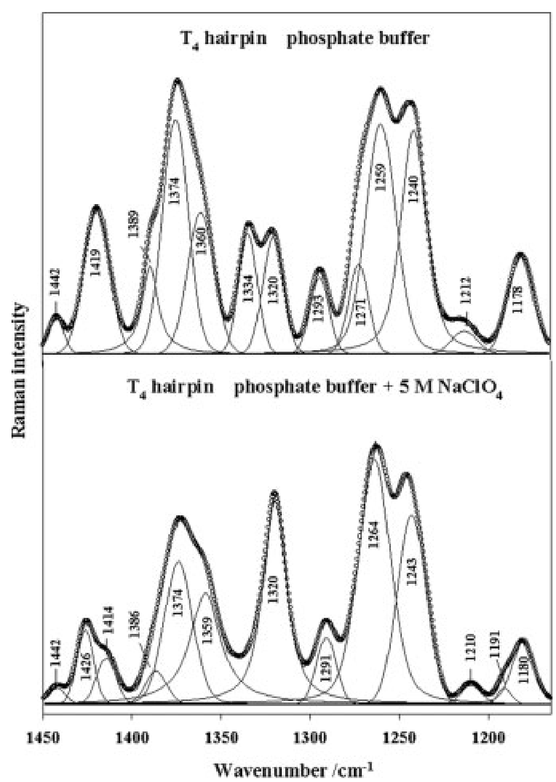

FIGURE 6 Band decomposition in the Raman spectra of T_4 hairpin in the 1450–1150-cm^{-1} spectral region. Top: T_4 hairpin with a B-form stem. Bottom: T_4 hairpin with a Z-form stem.

As an indicator of the melting effect in B-form stems, we note the considerable change of the C═O bond-stretch motions (1710–1650-cm^{-1} region), particularly the disappearance of the shoulder at ca. 1710 cm^{-1} (Figures 3 and 4), which is known as a marker of interbase hydrogen bonding in right-handed double helices. Less spectacular changes can be observed in the same region of the Raman spectra corresponding to the hairpins with Z-form stems (Figures 4 and 5).

Further Structural Information on the T_4 and A_4 Hairpins. Other questions to which we attempt to answer now, are those related to the conformation of the dT or dA nucleosides involved in the loops.

The dT and dA residues involved in the T_4 and A_4 hairpins with B-form stems seem to prefer C2′-*endo*/*anti* conformations. We mentioned above the existence of only C2′-*endo* sugars in these hairpins. The *anti* conformation of the bases (T or A) can be confirmed by the existence of a unique and well-resolved Raman band at 1420 cm^{-1} (Figures 3 and 4), marker of C2′-*endo*/*anti* nucleosides.[48] In Figure 3 (T_4 hairpin), we can recognize two vibrational modes appear-

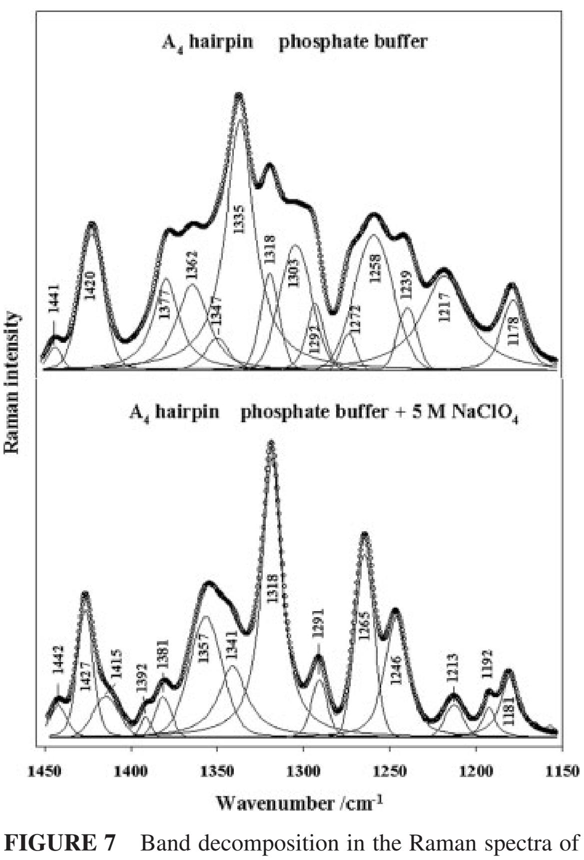

FIGURE 7 Band decomposition in the Raman spectra of A_4 hairpin in the 1450–1150-cm^{-1} spectral region. Top: A_4 hairpin with a B-form stem. Bottom: A_4 hairpin with a Z-form stem.

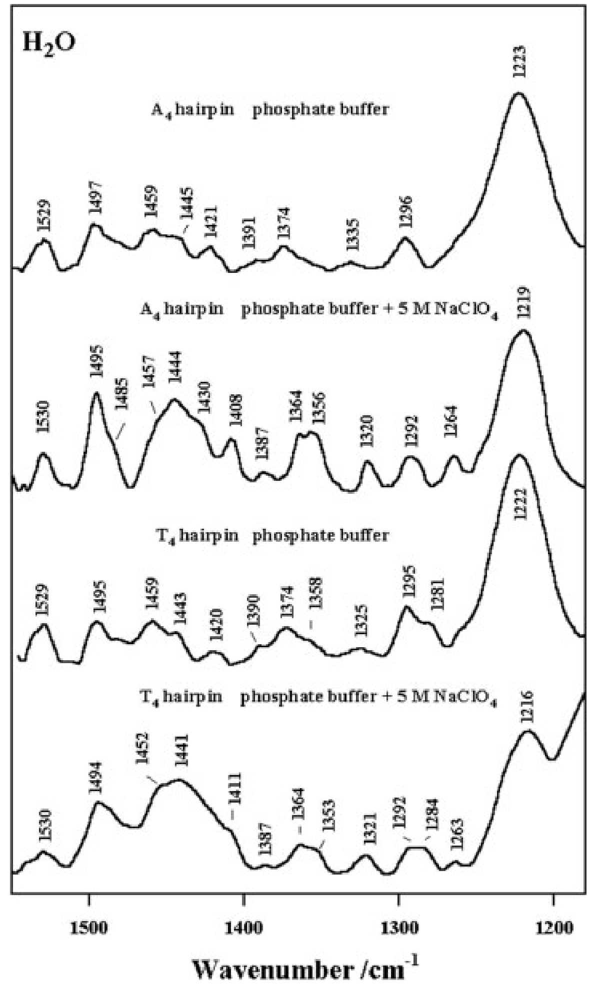

FIGURE 8 Room temperature FTIR spectra of H_2O solutions of the A_4 and T_4 hairpins observed in the 1550–1175-cm^{-1} spectral region. Oligonucleotide concentration was 5 m*M* at pH = 6.8. From top to bottom: A_4 hairpin formed in phosphate buffer (B-form stem), A_4 hairpin formed in phosphate buffer + 5*M* $NaClO_4$ (Z-form stem), T_4 hairpin formed in phosphate buffer (B-form stem), and T_4 hairpin formed in phosphate buffer + 5*M* $NaClO_4$ (Z-form stem).

ing as a weak band at 746 cm^{-1} and a shoulder at 667 cm^{-1} (located on the low wavenumber side of the dG residue marker at 680 cm^{-1}); both of them have been confirmed as markers of dT residues in C2′-*endo*/*anti* conformation.[25] In Figure 4 (A_4 hairpin with a B-form stem), the Raman spectrum displays in the 1400–1300-cm^{-1} spectral region, a general shape generally observed when the oligomer contains dA residues in *anti* orientation (the triplet at 1376, 1336, 1300 cm^{-1}).[25]

On the other hand, it can be confirmed that a part or all of the dT residues involved in the T_4 loop with a Z-form stem are in C3′-*endo*/*anti* conformation.

Note for this, the appearance of a shoulder at 1415 cm^{-1}, marker of C3′-*endo*/*anti* nucleosides[48] (Figure 5) and located at the low wavenumber side of the 1425 cm^{-1} (Z-helix marker).[48] In parallel, the intensity of the dT residues in C2′-*endo*/*anti* conformation (746 and 667 cm^{-1}) decreases considerably. Raman spectrum of the A_4 hairpin with a Z-form stem (Figure 4) gives markers confirming the C3′-*endo*/*syn* conformation for the loop dA residues. A unique band at 1427 cm^{-1} (Z-helix marker; C3′-*endo*/*syn* purines) is observed. In the 1400–1300-cm^{-1} region, the bands arising from the dA residues are completely changed compared to those observed in B-form stems (vide supra). In fact, the dA residue triplet confirming the anti orientation of adenine (1376, 1336, and 1300 cm^{-1}) are shifted to 1355 (superimposed undoubtedly with a dG residue Raman band observed at 1360 cm^{-1}), 1342, and 1319 cm^{-1} (superimposed with a dG residue Z-helix marker). Similar effects have been reported upon the observation of the B-to-Z transition of polyd(A-T).[27]

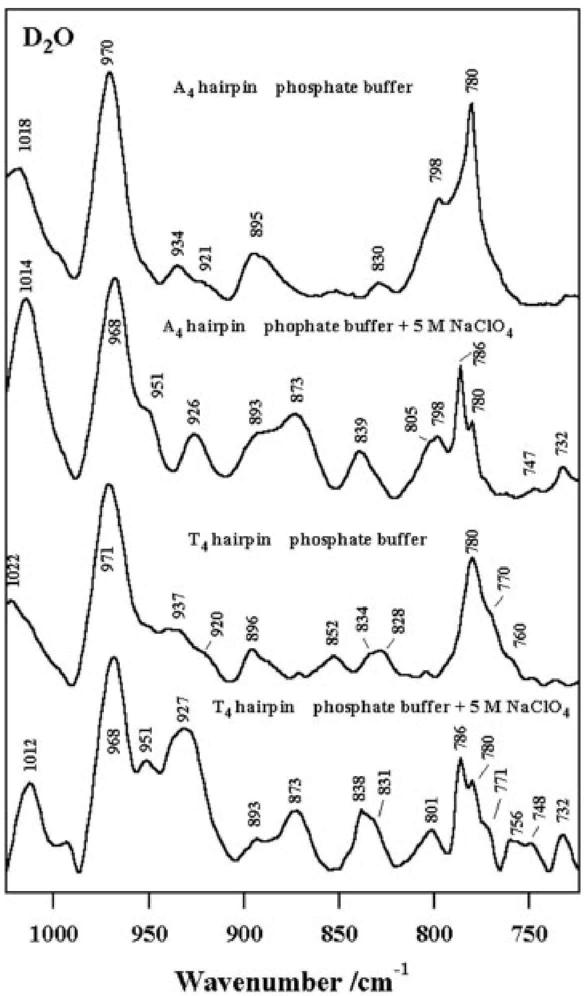

FIGURE 9 Room temperature FTIR spectra of D_2O solutions of the A_4 and T_4 hairpins observed in the 1025–725-cm^{-1} spectral region. Oligonucleotide concentration was 5 m*M* at pH = 6.8. From top to bottom: A_4 hairpin formed in phosphate buffer (B-form stem), A_4 hairpin formed in phosphate buffer + 5*M* $NaClO_4$ (Z-form stem), T_4 hairpin formed in phosphate buffer (B-form stem), and T_4 hairpin formed in phosphate buffer + 5*M* $NaClO_4$ (Z-form stem).

Analysis of a Possible Z-to-B Transition in T_4 and A_4 Hairpins by Means of CD and Raman Spectra

Partial Z-to-B transition has been reported by Benight et al.[40] in the T_4 hairpin upon heating, by means of CD and NMR data. We have attempted to analyze this transition by means of CD and Raman spectra recorded as a function of temperature in both T_4 and A_4 hairpins. CD spectra recorded as a function of temperature (10– 70°C) in the presence of 5*M* $NaClO_4$ are shown in Figure 10 for both hairpins. As mentioned above, the CD spectrum at 10°C corresponds to the hairpins with a Z-form stem. Upon heating, the Z-form signal suffers some significant changes: (i) a progressive red shift and signal decrease of the Z-form positive band, and (ii) a gradual decrease of the Z-form negative band. In other terms, the CD signal resembles that corresponding to an intermediate signal between B- and Z-forms (Figure 2). In order to explore evidence on the possible Z-to-B transition as a function of temperature, we scan again the 700–600 cm^{-1} of the difference Raman spectra of the T_4 (Figure 5) and A_4 (Figure 4) hairpins in the presence of 5*M* $NaClO_4$. These spectra show very well that at high temperature, the stem of the T_4 hairpin presents a partial Z-to-B transition (Figure 4): the intensity of the Z-form marker at 636 cm^{-1} is decreased, whereas a weak band at 680 cm^{-1} (B-form marker) appears. In the A_4 hairpin, the difference Raman spectrum (Figure 4) shows a considerable decrease of the 632 cm^{-1} without a notable increase at ca. 680 cm^{-1}. The absence of the Z-form Raman marker as well as the lack of a clear isoelliptic point on the CD spectra recorded as a function of temperature (Figure 10b) lead us to exclude a possible Z-to-B transition in this hairpin.

CONCLUSIONS

We have confirmed by means of optical spectroscopic (electronic and vibrational) techniques the formation of the T_4 and A_4 tetraloops hairpins. Both of these

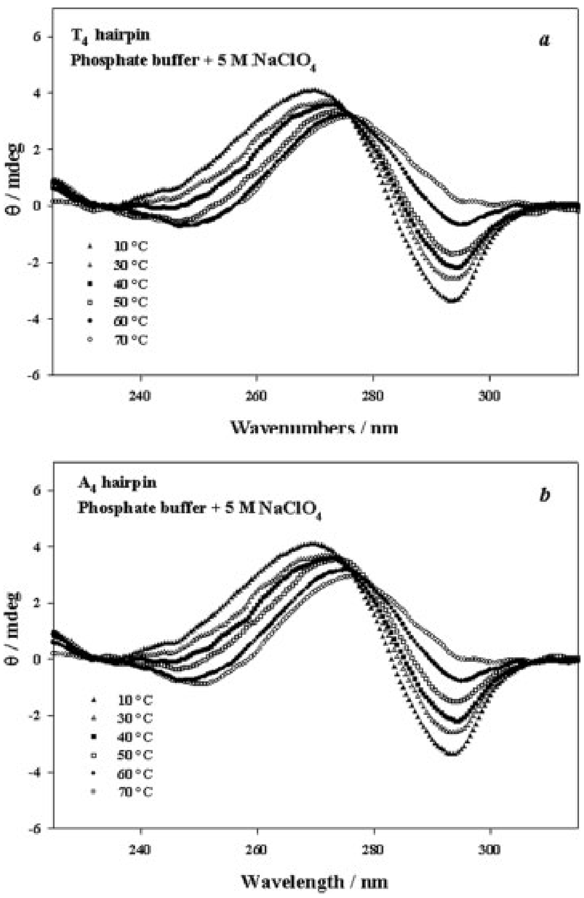

FIGURE 10 CD spectra of the T_4 (a) and A_4 (b) hairpins with a Z-form stem recorded in the temperature range between 10 and 70°C. Oligonucleotide concentration was 20 μM at pH = 6.8. To induce Z conformation in the stems, oligonucleotides were dissolved in phosphate buffer to which 5*M* $NaClO_4$ was added. Note that upon increasing temperature, the CD signal of both hairpins decreases without showing a clear Z-to-B transition (see also Figure 1).

hairpins have six GC base pairs in their stems. Although a right-handed stem can be formed in low ionic strength, even with no extra salt (NaCl) added to the phosphate buffer, the left-handed stem needs in contrast high ionic strength and the addition of non-routinely used salts, such as $NaClO_4$. On the basis of the present and previously published results, we can now claim that in the case of the T_4 hairpin, the stem length is the main element influencing the physicochemical conditions in which B-to-Z transition can appear: with ten GC base pairs the left-handed stem may be obtained in the presence of high concentration of NaCl and $MgCl_2$,[37] whereas with six GC base pairs 5*M* of $NaClO_4$ is needed (this work). The thermal stability of both tetraloop hairpins (T_4 and A_4) decreases drastically (ca. 17°C) upon B-to-Z transition of their stems, whereas in pentaloop hairpins (T_5 and A_5) the T_m difference between B- and Z-form stems does not exceed 4°C. The reverse transition (left- to right-handed) in the stem occurs in the T_4 hairpin when the temperature is increased. We assign this effect to the large amplitude motions of ClO_4^- ions (responsible for Z-helix formation). It should be noted that nothing is known up to now about the mechanism and dynamics of interactions of perchloride ions with DNA chains. Presumably, the Z-helix formation might be related to the interactions of ClO_4^- ions with dG residues, facilitating their transition to C3′-*endo*/*syn* conformation. Simultaneously, Na^+ ions might interact with DNA phosphate groups in order to induce the right-to-left-handed transition. No Z-to-B transition could be clearly evidenced in the A_4 hairpin. We conclude that the base composition of the tetraloops has a straight effect on the left- to right-handed transition of their stems.

BH acknowledges the Spanish Ministry of Education, Culture and Sport for a post-doctoral fellowship EX2001 12751081.

REFERENCES

1. Kleckner, N.; Chan, R. K.; Ty, B. K.; Botstein, D. J Mol Biol 1975, 97, 561–575.
2. Quigley, G. J.; Rich, A. Science 1976, 194, 796–806.
3. Maniatis, T.; Ptashne, M.; Backman, K.; Kleid, D.; Flashman, S.; Jeffrey, A.; Maurer, R. Cell 1975, 5, 109–113.
4. Rosenberg, M.; Court, D. Ann Rev Genet 1979, 13, 319–353.
5. Platt, J. R. Proc Natl Acad Sci USA 1955, 41, 181–183.
6. Vologodskii, A. V.; Lukashin, A. V.; Anshelevich, V. V.; Frank-Kamenetski, M. D. Nucleic Acids Res 1979, 6, 967–982.
7. Lilley, D. M. J. Proc Natl Sci USA 1980, 77, 6468–6472.
8. Lilley, D. M. J. Nucleic Acids Res 1981, 9, 1271–1289.
9. Panayotatos, N.; Wells, R. D. Nature 1981, 289, 466–470.
10. Haniford, D. B.; Pulleyblank, D. E. Nucleic Acids Res 1985, 13, 4343–4363.
11. Herbert, A.; Alfken, J.; Kim Y. G.; Mian I. S.; Nishikura, K.; Rich, A. Proc Natl Acad Sci USA 1997, 94, 8421–8426.
12. Oh, D. B.; Kim, Y. G.; Rich, A. Proc Natl Acad Sci USA 2002, 99, 1666–16671.
13. Brown, B. A., II.; Lowenhaupt, K.; Wilbert, C. M.; Hanlon E. B.; Rich, A. Proc Natl Acad Sci USA 2000, 97, 13532–13536.
14. Froelich-Ammon, S. J.; Gale, K. C.; Osheroff, N. J Biol Chem 1994, 269, 7719–7725.

15. Connelli, J. C.; de Leau, E. S.; Leach, D. R. F. Nucleic Acids Res 1999, 27, 1039–1046.
16. Li, J.; Bourdelat-Parks, B.; Boatright, J. H.; Wartell, R. M. Biochemistry 2003, 42, 10945–10954.
17. Samani, T. D.; Jollès, B.; Laigle, A. Antisense Nucleic Acid Drug Dev 2001 11, 129–136.
18. Vallone, P. M.; Paner, T. M.; Hilario, J.; Lane, M. J.; Faldasz, B. D.; Benight, A. S. Biopolymers 1999, 50, 425–442.
19. Moody, E. M.; Bevilacqua, P.C. J Am Chem Soc 2003, 125, 2032–2033.
20. Pohl, F. M.; Jovin, T. M. J Mol Biol 1972, 67, 375–396.
21. Pohl, F. M.; Ranade, A.; Stockburger, M. Biochim Biophys Acta 1973, 335, 85–92.
22. Thamann, T. J.; Lord R. C.; Wang, A. H. J.; Rich, A. Nucleic Acids Res 1981, 9, 5443–5457.
23. Benevides, J. M.; Thomas, G. J., Jr. Nucleic Acids Res 1983, 11, 5747–5761.
24. Wang, Y.; Thomas, G. A.; Peticolas, W. L. Biochemistry 1987, 26, 5178–5186.
25. Benevides, J. M.; Thomas, G. J., Jr. Biochemistry 1988, 27, 3868–3873.
26. Trulson, M. O.; Cruz, P.; Puglisi, J. D.; Tinoco, I., Jr.; Mathies, R. A. Biochemistry 1987, 26, 8624–8630.
27. Urpi, L.; Ridoux, J. L.; Liquier, J.; Verdaguer, N.; Fita, I.; Subirana, J. A.; Iglesias, F.; Huynh-Dinh, T.; Igolen, J.; Taillandier, E. Nucleic Acids Res 1989, 17, 6669–6680.
28. Abdelkafi, M.; Leulliot, N.; Ghomi, M.; Hervé du Penhoat, C.; Namane, A.; Gouyette, C.; Huynh-Dinh, T.; Baumruk, V.; Turpin, P. Y. J Mol Struct 1997, 408–409, 241–248.
29. Abdelkafi, M.; Ghomi, M.; Turpin, P. Y.; Baumruk, V.; Hervé du Penhoat, C.; Lampire, O.; Bouchemal-Chibani, N.; Goyer, P.; Namane, A.; Gouyette, C.; Huynh-Dinh, T.; Bednàrovà, L. J Biomol Struct Dyn 1997, 14, 579–593.
30. Abdelkafi, M.; Leulliot, N.; Baumruk, V.; Bednàrovà, L.; Turpin, P. Y.; Lampire, O.; Namane, A.; Gouyette, C.; Huynh-Dinh, T.; Ghomi, M. Biochemistry 1998, 37, 7878–7884.
31. Baumruk, V.; Gouyette, C.; Huynh-Dinh, T.; Sun, J. S.; Ghomi, M. Nucleic Acids Res 2001, 29, 4089–4096.
32. Leulliot, N.; Baumruk, V.; Abdelkafi, M.; Turpin, P. Y.; Namane, A.; Gouyette, C.; Huynh-Dinh, T.; Ghomi, M. Nucleic Acids Res 1999, 27, 1398–1404.
33. Leulliot, N.; Baumruk, V.; Gouyette, C.; Huynh-Dinh, T.; Turpin, P. Y.; Ghomi, M. Vibrat Spectrosc 1999, 19, 335–340.
34. Hernández, B.; Baumruk, V.; Leulliot, N.; Gouyette, C.; Huynh-Dinh, T.; Ghomi, M. J Mol Struct 2003, 651–653, 67–74.
35. Haasnoot, C. A.; den Hartog, J. H.; de Rooij, J. F.; van Boom, J. H.; Altona, C. Nucleic Acids Res 1980, 8, 169–181.
36. Haasnoot, C. A.; de Brui, S. H.; Berendsen R. G.; Jansen H. G.; Binnendijk, T. J.; Hilbers, C. W.; van der Marel, G. A.; van Boom, J. H. J Biomol Struct Dyn 1983, 1, 115–129.
37. Germann, M. W.; Schoenwaelder, K. H.; van de Sande, J. H. Biochemistry 1985, 24, 5698–5702.
38. Hare, D. R.; Reid, B. R. Biochemistry 1986, 25, 5341–5350.
39. Ikuta, S.; Chattopadhyaya, R.; Ito, H.; Dickerson, R. E.; Kearns, D. R. Biochemistry 1986, 25, 4840–4849.
40. Benight, A. S.; Wang, Y.; Amaratunga, M.; Chattopadhyaya, R.; Henderson, J.; Hanlon, S.; Ikuta, S. Biochemistry 1989, 28, 3323–3332.
41. Chattopadhyaya, R.; Ikuta, S.; Grzeskowiak, K.; Dickerson, R. E. Nature 1988, 334, 175–179.
42. Chattopadhyaya, R.; Grzeskowiak, K.; Dickerson, R. E. J Mol Biol 1990, 211, 189–210.
43. Wang, H. J.; Quigley, G. J.; Kolpak, F. J.; Crawford, J. L.; van Boom, J. H.; van der Marel, G.; Rich, A. Nature 1979, 282, 680–686.
44. Xodo, L. E.; Manzini, G.; Quadrifoglio, F.; van der Marel, G. A.; van Boom, J. H. Nucleic Acids Res 1986, 14, 5389–5398.
45. Xodo, L. E.; Manzini, G.; Quadrifoglio, F.; van der Marel, G. A.; van Boom, J. H. Biochemistry 1988, 27, 6321–6326.
46. Xodo, L. E.; Manzini, G.; Quadrifoglio, F.; van der Marel, G. A.; van Boom, J. H. Biochemistry 1988, 27, 6327–6331.
47. Puglisi, J. D.; Tinoco, I., Jr. Methods Enzymol 1999, 180, 304–325.
48. Thomas, G. J., Jr.; Wang, A. H. J. In Nucleic Acids and Molecular Biology; Eckstein, F., Lilley, D. M. J., Eds.; Springer-Verlag: Berlin Heidelberg, 1988; Vol 2, pp 1–30.
49. Wolk, S. K.; Hardin, C. C.; Germann, M. W.; van de Sande J. H.; Tinoco, I., Jr. Biochemistry 1988, 27, 6960–6967.

Reviewing Editor: Kenneth J. Breslauer